Electrical Properties of Sand–Clay Mixtures Containing Trichloroethylene and Ethanol

Jeffery J. Roberts and Dorthe Wildenschild*
Lawrence Livermore National Laboratory, L-201, P.O. Box 808, Livermore, Calif. 94551-0808, USA

ABSTRACT

A series of laboratory experiments that measured electrical properties and permeability was performed on carefully characterized sand–clay mixtures. Different mixtures and configurations of quartz sand and 10% Na-montmorillonite clay were investigated using solutions of NaCl, $CaCl_2$, and deionized water. A sample containing 10% dispersed clay was also studied using fluids containing 20- and 500-ppm trichloroethylene (TCE). Each sample's electrical properties after fluid saturation were measured at frequencies between 10^{-2} and 10^6 Hz by using the four-electrode method with Ag–AgCl inner electrodes at room temperature and 412-kPa confining pressure, which corresponds to a soil depth of 15–20 m. Our results show that adding TCE had a small effect on electrical resistivity: resistivity was greater at higher concentrations of TCE. The influence of TCE on electrical properties was most prominent in plots of loss tangent as a function of frequency. These plots showed that loss-tangent peaks occurred at ~200 Hz and that peak and peak frequency heights were smaller at higher concentrations of TCE. Additional experiments were performed on a sample that contained a distinct clay layer parallel to the current flow. The electrical properties of the sample were measured as it was saturated with deionized water and $CaCl_2$ solutions, and as an ethanol–water mixture (80:20) was flowed through the sample. Resistivity increased by about a factor of 4 as the ethanol mixture replaced the water solution. Nondestructive x-ray imaging of the sample at various stages of dewatering indicated a decrease in the thickness of the clay layer as more pore volumes of ethanol–water were flowed. Our results show that electrical measurements are useful tools for characterizing porous rocks and soils and that it is feasible to remotely detect the presence and follow the transport of contaminants such as TCE in the subsurface.

Introduction

Background

Frequency-dependent electrical measurements are a useful nondestructive method for characterizing porous rocks and soils. The conduction of electricity through porous media occurs primarily by the movement of ions through bulk-saturating fluid. In addition, conduction takes place as adsorbed ions move along the surfaces of pores and cracks. Thus, the conductivity of a porous medium is related to microstructural properties such as the porosity, pore geometry, and surface morphology of the mineral grains lining the pores, as well as the dielectric properties of the mineral grains and pore fluid. Electrical conduction is also a function of the prevailing fluid saturation. For brine-saturated porous materials, Archie (1942) proposed the following relationship between bulk and fluid conductivities:

$$\sigma_{bulk} = \sigma_{fluid} a \phi^m \tag{1}$$

where σ_{bulk} is the electrical conductivity of the porous medium, σ_{fluid} is the electrical conductivity of the saturating fluid, ϕ is the porosity, and a and m are parameters that are assumed to be constant for specific rock types. The ratio $\sigma_{fluid}/\sigma_{bulk}$ is called the formation factor F. In Eq. (1), the contribution of surface conduction to bulk conduction is assumed to be negligible.

However, when surface conduction is important, Archie's law must be modified (Johnson *et al.*, 1986; Waxman and Smits, 1968; Sen *et al.*, 1988; Sen and Goode, 1992) because the σ_{bulk} and σ_{fluid} variables are no longer purely proportional; instead, they exhibit a linear dependence that has an intercept on the ordinate axis. Johnson *et al.* (1986) defined a length parameter Λ, which is a weighted volume-to-surface-area ratio (a measure of the dynamically interconnected pore size), as

$$\frac{\Lambda}{2} = \frac{\int |E(r)|^2 dV_p}{\int |E(r)|^2 dS}, \tag{2}$$

where $E(r)$ is the electric potential field at point r, V_p is the pore volume, and S is the surface area (*i.e.,* the pore–solid interface). The Λ parameter, which is expressed in units of length, characterizes the geometry of a porous medium and is transferable from one experiment to another for specific media. Equation (2) is valid for materials with insulating

* Currently at Oregon State University, Department of Geosciences, 104 Wilkinson Hall, Corvallis, OR 97331-5506, USA.

grains that are coated with appreciable amounts of clay minerals (Johnson *et al*., 1986).

In the case where dry clays are saturated with brines, the counter ions hydrate and become mobile within a layer. These counter ions usually balance out charged impurities by bonding to their external surfaces, and the resulting surface conduction is due to their acting in parallel with the ionic conduction associated with the brine. For relatively high-salinity pore fluids, the following linear relationship has been derived (Johnson *et al*., 1986):

$$\sigma_{\text{bulk}} = \frac{1}{F}\left(\sigma_{\text{fluid}} + \frac{2\Sigma_s}{\Lambda}\right), \tag{3}$$

where Σ_s is the surface conductivity. When σ_{fluid} and σ_{bulk} are plotted on a linear scale, the slope equals the reciprocal of the formation factor F, and the intercept with the ordinate axis equals $2\Sigma_s/F\Lambda$.

Previous Work

Previous work by Wildenschild *et al*. (1999, 2000) demonstrated the influence of various microstructural properties, such as clay content and configuration, on electrical properties. Wildenschild *et al*. determined formation factors, Λ parameters, and surface conductances for a number of different configurations containing 0 to 10% clay. The configurations included dispersed mixtures, discrete clay clusters, and arrangements of distinct layers of clay within a sand matrix. They found that Eq. (3) described conduction for a wide range of parameters, including fluid salinity, clay content, and surface conductance. This paper presents additional work on the samples studied by Wildenschild *et al*. using pore fluids that contained small amounts (<500 ppm) of trichloroethylene (TCE) or ethanol–water mixtures.

Work on clay-bearing materials containing organic compounds has been performed previously, and a brief review of this work follows: Olhoeft and King (1991) reported complex resistivity measurements on synthetic clay–toluene mixtures. They found a resistivity increase (~10 to 30%) and a larger (negative) phase angle for samples containing up to 20% toluene. The resistivity difference was greatest at frequencies below ~100 Hz, and the phase difference was greatest between 1 and 100 Hz. Separate work by Chan *et al*. (2000) on sand–clay mixtures demonstrated that noncontaminated samples show little frequency dependence and follow Archie's law. However, when TCE was present in a 100% sand sample, Chan *et al*. found that Archie's law did not apply. Resaturating the contaminated sample with brine produced anomalous results, which were attributed to the incomplete removal of TCE.

A comprehensive set of experiments on prepared and natural clay-bearing samples was performed by Jones (1997) as part of his thesis work. In these experiments, Jones measured complex electrical properties from 10^{-3} to 10^{6} Hz, while varying solution types and concentrations. Measurements were taken on samples containing a variety of organic contaminants, including TCE, tetrachloroethylene, ethylene glycol, and phenol. Jones observed changes in the nonlinear character of the complex response that were attributable to chemical reactions between the clay and the organic contaminants. In addition, spectral alterations were observed to take place for as long as one month, at which point equilibrium had not yet been established. Jones suggested that field electromagnetic (EM) data can be used to locate contaminated regions by identifying changes in nonlinear response.

This paper is largely an experimental results paper in which we show that small amounts of TCE affect the electrical response of sand-clay mixtures and that the changes are most prominent in plots of loss tangent as a function of frequency. We also report changing electrical properties as ethanol–water mixtures are flowed through clay-bearing samples and use x-ray imaging to quantitatively determine clay-layer shrinkage due to dewatering. There is a considerable need for additional experiments aimed at verifying the results and at identifying and understanding the physical mechanisms causing the observed electrical responses.

Experimental Details

Sample Preparation and Characterization

Pure silica sand (F-50 Ottawa sand from U.S. Silica) and Na-montmorillonite (Wyoming bentonite) were used to build the samples in our experiments. The Ottawa sand had grain sizes between 74 and 420 μm, a median diameter (d_{50}) of 273 μm, and a particle density of 2.66 g/cm^3. To create the dispersed-clay samples, dry sand and clay were mechanically mixed and packed into sample holders made of 5.08-cm-diameter, heat-shrink tubing, with sintered Hasteloy frits at both ends that provided support, allowed fluid flow, and served as current electrodes. In the case of the parallel-clay-layer sample, dry sand was packed around a vertical clay layer so that the sand and clay layer were in contact with both end frits.

The height of each sample was 3.8 cm, and additional heat-shrink material was used to position two AgCl-coated, silver-wire electrodes in the casing 0.63 cm from either end of each sample. The electrochemically coated Ag–AgCl wires served as potential electrodes. Platinum electrodes were unsuitable for our experiments because hydrolysis at the metal–water interface of platinum electrodes would produce unreliable measurements. The AgCl-coated Ag wires alleviated this problem by providing a means of ionic exchange with the saturating solution. After each sand–clay mixture was packed between the frits, the tubing was heated, causing it to shrink and rigidly support each unconsolidated sample.

Pore Fluids

Each sample was saturated with saline fluids of varying concentrations, ranging from 0.0005 N to 0.75 N of $CaCl_2$ (0.05 to 64 mS/cm). Electrical measurements were then made using deionized water, and the results were reported in Wildenschild *et al*. (2000). Solutions of 600-μS/cm NaCl (~0.0035 N) were prepared that contained 0, 20, and 500 ppm TCE, below the TCE solubility limit of 1099 ppm in water at 20°C. These solutions were used as pore fluids in the 10% dispersed clay sample. Additional experiments were performed with an 80:20 mixture of ethanol and deionized water that had a conductivity of ~0.76 μS/cm. This fluid was flowed through the sample containing the parallel clay layer.

Apparatus and Measurement Procedures

The experimental setup consisted of four major components: the sample, the sample holder with pressure controls, the electrical-measurement system, and the fluid-flow system (Fig. 1; Wildenschild *et al*., 2000). Each sample was placed in a Hassler sleeve that was used to control pore pressure. The Hassler sleeve was then placed between insulating Delrin end caps, which had openings for fluid inlet and outlet and for the electrical input and output voltage leads. During the experiments, applied end-load and in-load pressures from air-actuated cylinders held the Hassler sleeve in place. End-load, in-load, and confining pressures of 60 psi (418 kPa) were used in all experiments. The various loads simulated shallow burial and ensured that the sample was hydraulically sealed in the holder (*i.e.,* that sidewall flow was avoided).

Electrical Measurements

Each time a fluid was pumped through a sample, frequency-dependent electrical properties were measured using the four-electrode method (Olhoeft, 1985). Impedance magnitude ($|Z|$), phase angle (ϕ), electrical resistance (R), and capacitance (C) were measured with an HP4284A LCR meter during flow and at hydraulic equilibrium. Complex impedance spectra over a wider range of frequencies (10 mHz to 1 MHz) were measured using a Solartron 1260A impedance analyzer. Tests on a fluid-filled dummy sample holder were performed to test the accuracy of the system and to calculate carefully the geometrical factor of the sample holder at run conditions. It was found that the frequency-dependent electrical response of dilute saline solutions was nearly independent of frequency from the lowest frequency of measurement to $\sim 10^4$ Hz. Above this frequency the system capacitance, which was determined to be <30 pF, contributed to the response. The data presented here are uncorrected for this capacitance.

Complex impedance has two parts—real and imaginary—and is described by the following equation:

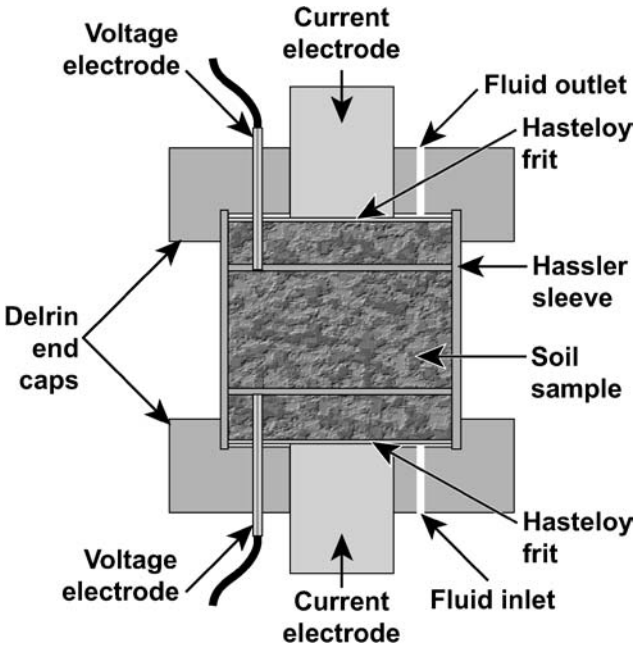

Figure 1. The experimental apparatus used to confine pressure, control fluid flow, and measure impedance.

$$Z^* = Z' - jZ'', \tag{4}$$

where Z' represents the real impedance, Z'' represents the imaginary impedance, and $j = \sqrt{-1}$. Resistivity (ρ) is the specific property that takes into account the sample's geometry and is given by

$$\rho^* = Z^*\left(\frac{A}{l}\right), \tag{5}$$

where A/l is the area:length ratio of the cylindrically shaped sample. Electrical conductivity (σ) is the reciprocal of the resistivity. The relationship between dielectric permittivity (κ) and the impedance of a conducting material is described in Eq. (6):

$$\kappa^* = \kappa' - j\kappa'' = (j\omega C_0 Z^*)^{-1}, \tag{6}$$

where κ^* is the dielectric permittivity divided by the permittivity of free space (ε_0) and has a value of 8.854×10^{-12} F/m, ω is the angular frequency, and C_0 is the capacitance of the empty cell in a vacuum ($C_0 = \varepsilon_0 A/l$). The loss tangent parameter ($\tan\delta$) is defined as follows:

$$\tan\delta = \frac{\sigma' - \varepsilon''\omega}{\sigma'' + \varepsilon'\omega} \approx \frac{\sigma'}{\sigma''}. \tag{7}$$

The loss tangent approximates the conductivity ratio (or the inverse of the phase angle) when angular frequency (ω) is zero and conduction currents dominate displacement currents (Ward and Hohmann, 1987). The loss tangent is also called the dissipation factor and measures the energy transferred to the material from the electric field, primarily

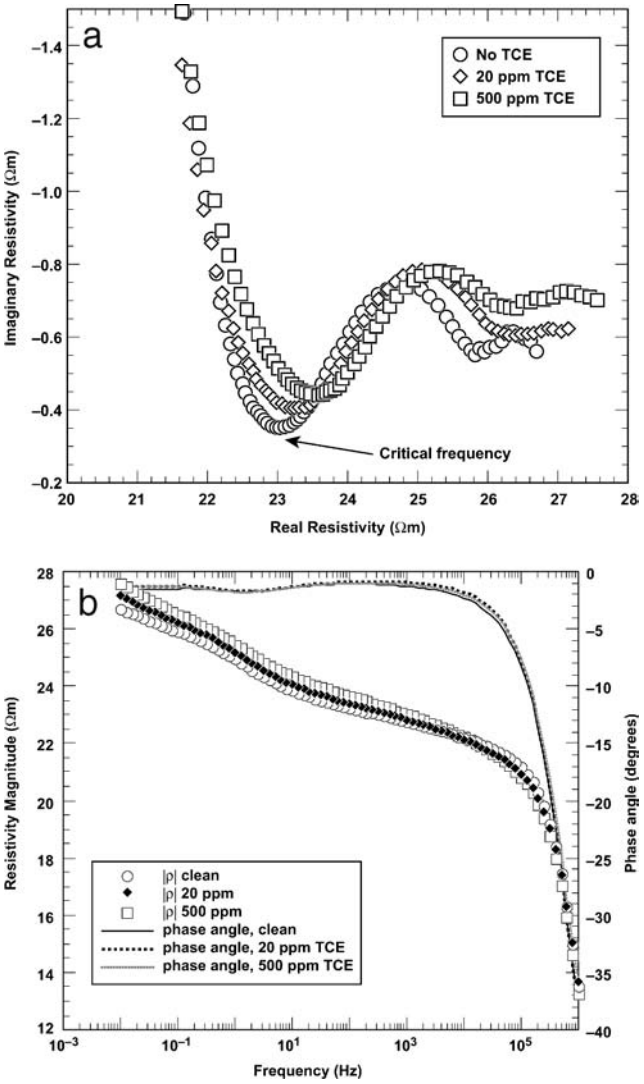

Figure 2. Plots showing (a) imaginary vs. real resistivity and (b) resistivity magnitude and phase angle vs. frequency in the 10% dispersed bentonite clay sample after being saturated in solutions with varying concentrations of TCE.

through friction associated with the movement of ions and dipoles.

Results and Discussion

Electrical Measurements on Samples Containing TCE

The electrical impedance of the 10% dispersed bentonite clay sample depended on the amount of TCE present. Figure 2a plots imaginary versus real resistivity as a function of TCE content. Portions of three impedance arcs are visible in Fig. 2a, and the first two higher-frequency arcs widen, indicating that higher concentrations of TCE were accompanied by greater resistance. Figure 2b shows

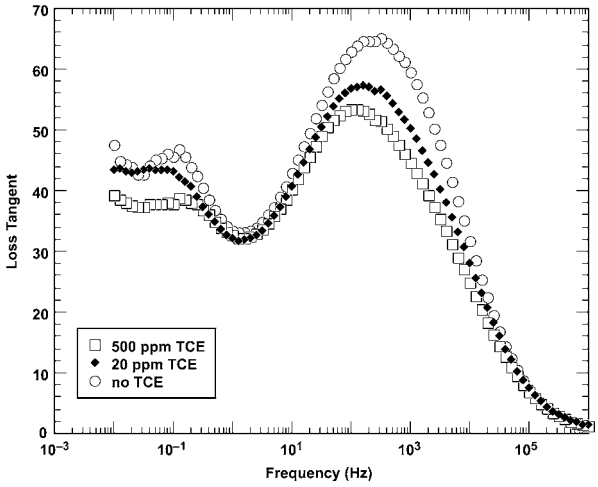

Figure 3. Plot showing loss tangent vs. frequency for the 10% dispersed bentonite clay sample after being saturated in solutions with varying concentrations of TCE.

impedance magnitude and phase angle plotted as a function of frequency for the same samples as in Fig. 2a. The critical frequency, the frequency where the minimum phase angle occurs (Dias, 2000), was lower by a factor of about 2.5 for the sample containing 500 ppm TCE when compared with the clean sample. This is most readily observed in Fig. 2a by observing where imaginary resistivity comes closest to the real axis.

The loss tangents for the three experiments are plotted in Fig. 3. We found that differences in electrical response were most apparent in this type of plot. The most prominent feature in Fig. 3 is the loss-tangent peak that occurred between 100 and 1,000 Hz; this loss-tangent peak decreased in magnitude and shifted to a slightly lower frequency at higher concentrations of TCE. The frequency of the largest loss-tangent peak coincided with the critical frequency.

The highest frequency-impedance arc in Fig. 2a shows that the sample containing 500 ppm TCE exhibited 5% greater resistance than the clean sample. An increase in resistance might be expected as the conductive fluid is displaced by the more resistive TCE. However, in our experiment the amount of TCE is below the solubility limit and within the resolution of the conductivity meter all the solutions containing TCE had the same measured electrical conductivity. The change in resistance was greater than would be expected from the amount of TCE that was added, indicating the presence of an additional mechanism. The magnitude of the loss-tangent peak in Fig. 3 was about 17% smaller for the sample containing 500 ppm TCE than for the clean sample. One possibility is that this effect may have been partially caused by a change in the exchangeability of the clay because of the presence of TCE. However, other electrochemical reactions may also have contributed to this effect.

Equivalent Circuit Fitting of Impedance Data

Additional information regarding how each sample responds to the presence of TCE can be obtained by performing equivalent circuit analysis of the impedance data (*i.e.,* Macdonald, 1985; Knight, 1984). Such an analysis can provide insight into the nature of the mechanisms causing the observed electrical response. Numerous equivalent circuits can be used to fit a specific data set and a chosen equivalent circuit may not be the correct choice. However, the analysis does provide a quantitative basis for different mechanisms and their relaxations that may help understand the relevant physical processes. For the responses here a simple equivalent circuit of three parallel-resistor, constant-phase elements (R-CPE) in series is adequate to fit the data closely using a non-linear least squares fitting routine (CNLS). The constant phase element has an electrical response of the form

$$Z_{CPE}^* = (Y_{CPE}^*)^{-1} = (j\omega\tau)^{-\alpha} \tag{8}$$

where α is a frequency-independent parameter that relates to the angle of depression of the impedance arc and τ is the time constant of the relaxation mechanism. For a CPE in parallel with a resistor the response is given by

$$Z_{ZARC}^* = \frac{R}{1 + (j\omega\tau)^{\alpha}} \tag{9}$$

where Z_{ZARC}^* is the complex impedance of an arc depressed in the complex impedance plane. For $\alpha = 1$, the CPE is an ideal capacitor, the impedance arc is not depressed (center lies on the real axis), and there is a single time constant τ. For $\alpha = 0$, the CPE is an ideal resistor and there is no imaginary component (Roberts and Lin, 1997). When the center of the impedance arc falls below the real axis the time constant is not single-valued but has a distribution.

An example of this approach is seen in Fig. 4 where both the data and the CNLS fit are shown. Table 1 has the parameter values from the CNLS fitting using the three R-CPE elements arranged in series. Element 1 is the highest-frequency element, followed by element 2, and element 3 is the lowest-frequency element.

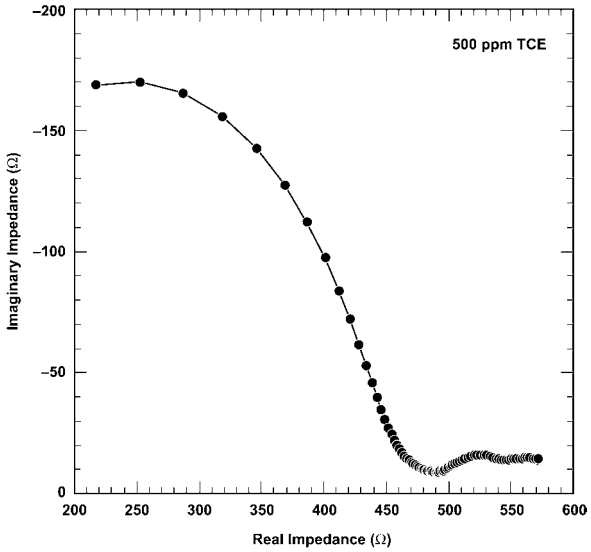

Figure 4. Impedance diagram for sample containing 500 ppm TCE (points) and the equivalent circuit fit (line). Equivalent circuit model contains three R-CPE elements in series as discussed in text. Values for circuit parameters are listed in Table 1.

The resistance of the high-frequency impedance arc is actually observed to decrease slightly with the addition of TCE to the pore fluid. The lower-frequency impedance arcs increase resistance with the addition of TCE. The intermediate-frequency arc shows the strongest effect, an increase in resistance of approximately 24%. The 20- and 500-ppm TCE samples have nearly the same resistance for this circuit component. The resistors R1 and R2 both exhibited this behavior—that the presence of TCE seemed to alter the value of the circuit component from the clean sample

Table 1. Equivalent circuit fitting parameters.

Sample/circuit component	Clean sample	20 ppm TCE	500 ppm TCE
R1 (ohms)	358.4 ± 9.4	336.2 ± 7.7	337.7 ± 7.1
R2 (ohms)	115.5 ± 7.4	142.8 ± 5.9	142.9 ± 5.4
R3 (ohms)	96.7 ± 3.9	102.4 ± 3.8	122.9 ± 4.9
CPE-1	1.6 e-9 ± 1.2 e-10	1.7 e-9 ± 1.2 e-10	1.8 e-9 ± 1.2 e-10
CPE-2	3.8 e-5 ± 2.5 e-5	4.0 e-5 ± 1.7 e-5	3.3 e-5 ± 1.2 e-5
CPE-3	6.6 e-3 ± 2.9 e-4	6.6 e-3 ± 2.6 e-4	7.2 e-3 ± 2.7 e-4
α-1	0.929 ± 0.007	0.926 ± 0.006	0.926 ± 0.006
α-2	0.328 ± 0.036	0.317 ± 0.023	0.343 ± 0.018
α-3	0.363 ± 0.013	0.361 ± 0.012	0.314 ± 0.011
Chi-Squared	9.16 e-05	7.13 e-05	5.77 e-05

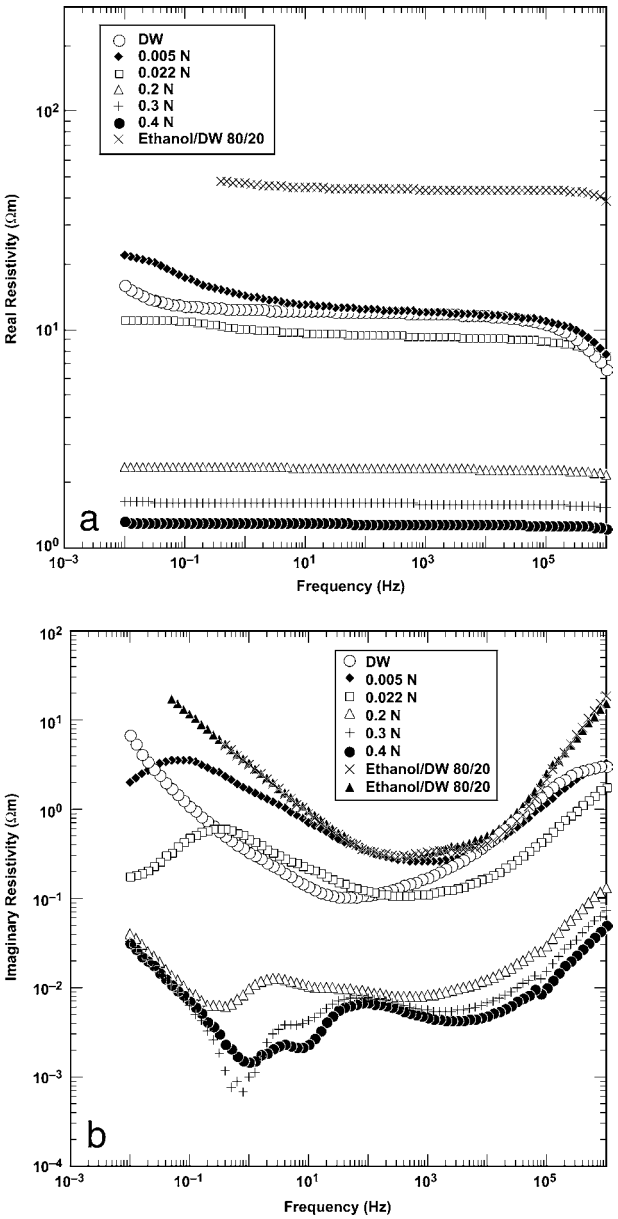

Figure 5. Real (a) and imaginary (b) resistivity for the parallel clay layer sample for a range of saturating solutions. The addition of the ethanol mixture increased the resistivity about a factor of 5 over the most resistive pore fluid.

value, and did not vary with either the 20- or 500-ppm TCE samples.

The lower-frequency arcs are observed to have a much slower time constant (R·CPE) than the higher-frequency arc and also have a center well below the real impedance axis. This indicates a strong distribution of relaxation times and significant overlap of the impedance arcs. It is probable that the high-frequency arc has a parallel component that is lumped under the present circuit configuration. It is not possible to evaluate this possible mechanism with the current data set.

Further work is required to identify the physical mechanism(s) causing the observed changes in electrical properties from a small addition of TCE to the saturating fluid. Even though the specific mechanism causing the change in electrical response is unknown, these results indicate, in accordance with Jones (1997), that it may be possible to use the response to locate small amounts of contamination in field sites using EM methods.

Electrical Measurements on Samples Containing Ethanol

The behavior of clay-bearing soil that contains ethanol is of interest in environmental remediation because ethanol dewaters clays and causes them to contract. One typical drawback to pump-and-treat remediation of clay-bearing soils containing organic contaminants is the amount of time it takes for contaminants to diffuse to permeable flow channels. However, one hypothesis suggests that ethanol not only dewaters clay but also causes microcracks in clay layers, which provides a shorter pathway for the migration and removal of contaminants (Brown and Thomas, 1987; Anandarajah, 2003). Because of the interest in the potential use of ethanol for environmental remediation, we measured the electrical properties of a sand–clay sample containing a clay layer that was parallel to the direction of fluid flow and electrical measurement. Electrical impedance measurements were made as deionized water and $CaCl_2$ solutions ranging from 0.005 to 0.4 N saturated the sample (Wildenschild *et al.*, 2000) and as an 80:20 ethanol–water mixture (~0.76 μS/cm) was flowed through the sample at a rate of 5 ml/h.

The electrical resistivity of the parallel-clay-layer sample decreased as the salinity of the $CaCl_2$ fluid increased (Figs. 5a and 5b). However, this effect was not as strong as the effect observed in the 10% dispersed clay samples (Wildenschild *et al.*, 2000; and Figs. 6a and 6b). This result can be attributed to the fact that the parallel-clay-layer sample had the highest surface conductance (2.45 μS) of the samples studied in our experiments and was, due to its clay-layer geometry, fairly conductive, even for the most dilute saturating solutions. For both samples the real resistivity is fairly constant from 0.1 Hz to 100 kHz (Figs. 5a and 6a). The imaginary resistivity for both samples displays a stronger frequency-dependent behavior. For the parallel clay layer sample the imaginary resistivity response for the ethanol/water mixture is similar to that of the most dilute $CaCl_2$ solutions, particularly between 10 Hz and 10 kHz (Fig. 5b). The higher-salinity solutions display a stronger frequency dependence (imaginary resistivity) than the dilute solutions at frequencies below approximately 10 Hz.

The loss tangents for the 10% dispersed-clay sample (Fig. 7a) displayed more variation with frequency than the loss tangents for the parallel-clay-layer sample (Fig. 7b). At greater salinity concentrations, the loss tangents for the 10%

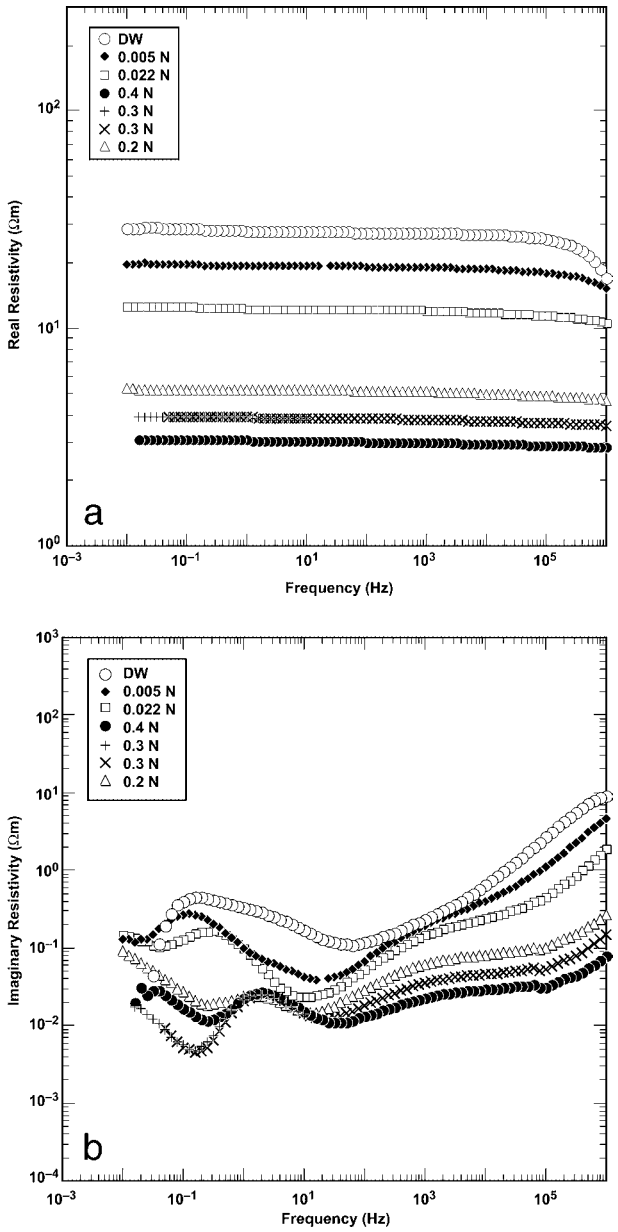

Figure 6. Real (a) and imaginary (b) resistivity for the 10% dispersed clay sample for a range of saturating solutions.

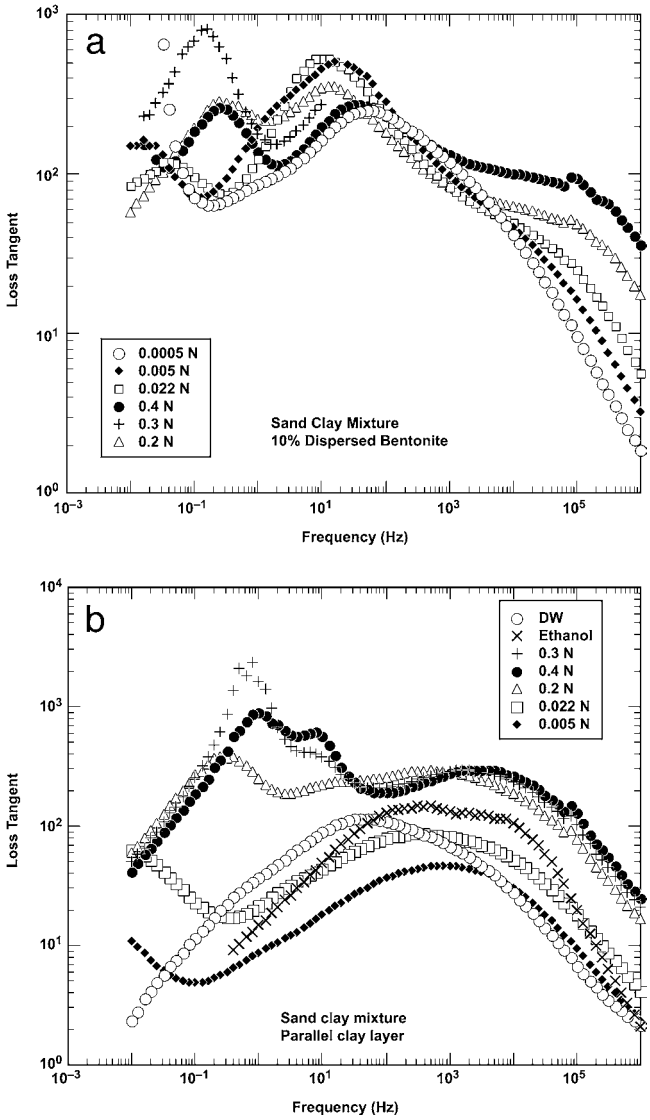

Figure 7a. Plot showing loss tangent vs. frequency for the 10% dispersed bentonite clay sample after being saturated in solutions with varying concentrations of $CaCl_2$. Figure 7b. Plot showing loss tangent vs. frequency for the parallel-clay-layer sample after being saturated in deionized water (DW), the ethanol–water mixture, or solutions with varying concentrations of $CaCl_2$.

dispersed-clay sample were higher and showed more peaks or peaks shifted to lower frequency. These low-frequency peaks occurred between 0.1 and 100 Hz and were absent when the 10% parallel-clay-layer sample was saturated with either deionized water or the ethanol–water mixture.

As the ethanol–water mixture was flowed through the parallel-clay-layer sample, impedance increased by about a factor of 4 over the impedance resulting from the 0.022 N $CaCl_2$ solution. Additional flow of the ethanol–water mixture up to 10 pore volumes continued to increase the impedance. After 15 pore volumes, the fluid flow was stopped, and impedance subsequently decreased over time. The loss tangent for the parallel-clay-layer sample saturated with the ethanol–water mixture showed a single peak centered near 500 to 1,000 Hz (Fig. 7b). As more of the ethanol–water mixture was flowed, the peak first decreased in magnitude and then increased. After about 10 pore volumes had been displaced, a second peak or shoulder appeared at a higher frequency. The noisiness of the response increased over time.

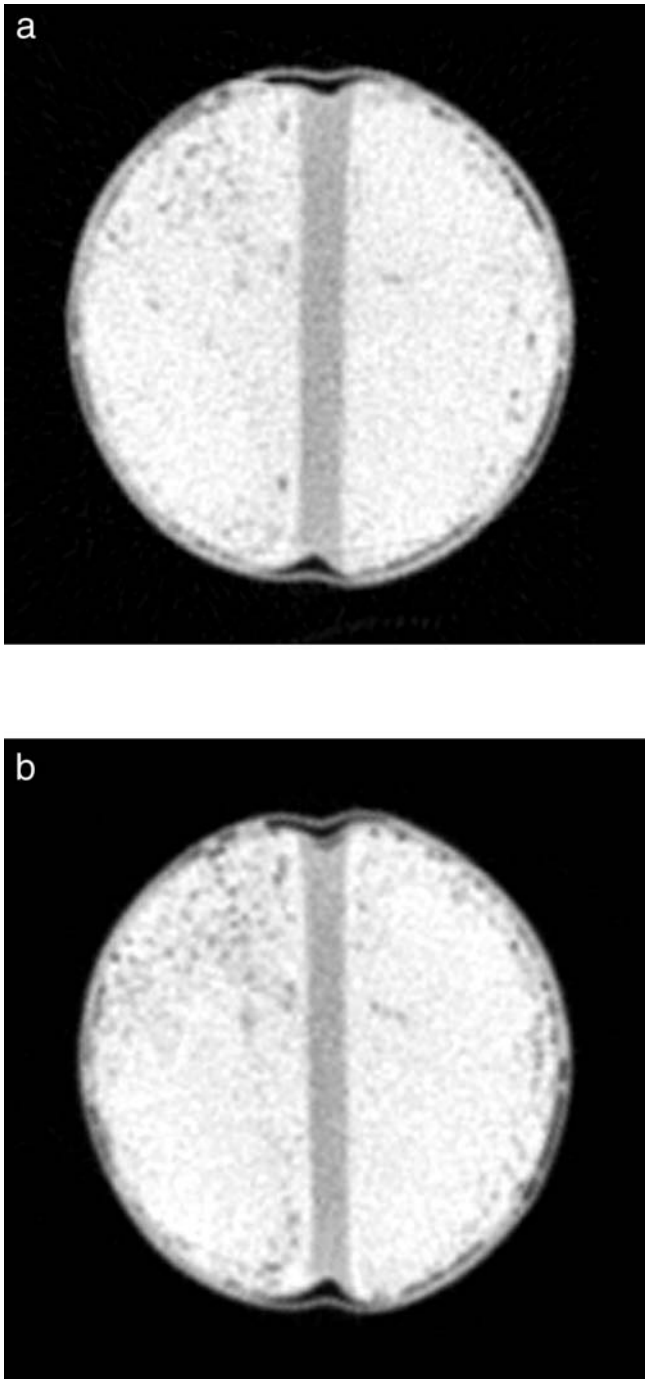

Figure 8. Reconstructed x-ray computed tomography slices of the parallel-clay-layer sample (a) prior to and (b) after ~10 pore volumes of ethanol–water flow. In these images, a brighter shade is more attenuating than a darker shade. The gray, vertical stripe is the clay layer that changed thickness after ethanol–water flow. The sample was ~5.08 cm in diameter, and each pixel in the images measures ~390 × 390 μm.

X-Ray Images

The parallel-clay-layer sample was x-rayed periodically during the ethanol–water flow portion of the experiment. Flow was stopped periodically, and the sample was x-rayed to gain information about the thickness and integrity of the clay layer. The x-ray procedure that we followed was very similar to the procedure described by Roberts and Lin (1997). A 160-kVp linear source was used to x-ray the sample as it was rotated and translated vertically through the beam. A two-dimensional photodiode linear-array detector was then used to convert and store the digital signal. Finally, the independent views (radiographs) were reconstructed into a series of tomographic slices, which showed the x-ray attenuation of the sample as a function of time. Some systems in our laboratory can achieve spatial resolutions of about 5 μm; however, the spatial resolution for the system used in this experiment was about 390 μm. Higher-resolution scans are required to image the microcracks in the clay layer.

Reconstructed tomographic cross sections of the cylindrical sample are shown in Figs. 8a and 8b. Figure 8a shows the sample prior to ethanol–water flow, and Fig. 8b shows the sample after ~10 pore volumes of the 80:20 ethanol–water mixture have flowed through the sample. The primary feature to note is the thickness of the clay layer (the gray, vertical stripe in the center of each image) before and after the ethanol–water flow. Although the spatial resolution of these images is insufficient to image the cracking in the clay, the effect of dewatering can be readily seen as a reduction in clay-layer thickness.

Figures 9a and 9b show averaged lines of attenuation across (Fig. 9a, horizontal) and within the clay layer (Fig. 9b, vertical). Five lines were averaged to smooth the data. The curves are labeled sequentially from earlier to later in the experiment and correlate to the amount of the ethanol–water mixture that has flowed through the sample. Figure 9a shows the width of the clay layer decreasing, and Fig. 9b shows the attenuation of the clay layer increasing as the total flow increased over time. Overall, the thickness of the clay layer decreased by 25–40% after approximately 10 pore volumes of fluid flow.

Conclusions

Our experiments investigated the influence of TCE (20- to 500-ppm) on the complex impedance of sand–clay samples. The presence of TCE had only a minor effect on the electrical resistivity. A more pronounced effect was observed in the loss tangent, with a peak centered near 200 Hz that shifted to slightly lower frequency and decreased in height at higher concentrations of TCE. Additional experiments are necessary to verify and determine the physical cause of the observed response. Electrical experiments were performed on a sample containing a parallel clay layer as an

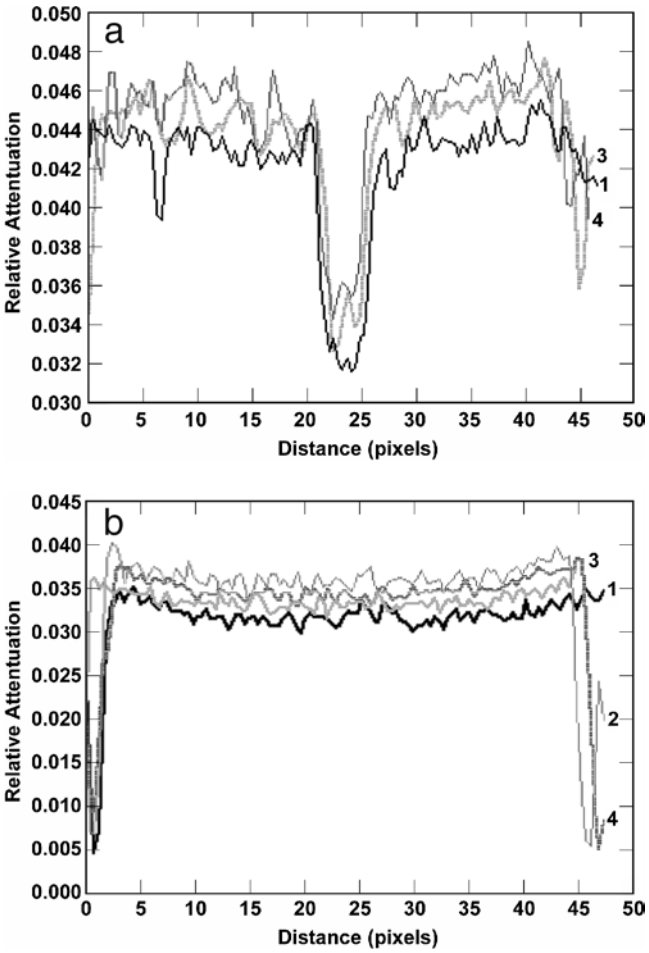

Figure 9. Relative attenuation vs. distance across the parallel-clay-layer sample as a function of total flow of the 80:20 ethanol–water mixture over time. As total flow increased over time, (a) attenuation across the clay layer indicated a shrinking layer, and (b) attenuation within the clay layer showed increased attenuation.

ethanol–water mixture was displaced through the sample. Resistivity in this sample increased by as much as a factor of 4 as the ethanol–water mixture replaced the 0.022 N $CaCl_2$ solution. X-ray imaging during the dewatering experiment quantified the change in the sample's clay layer, which decreased in thickness by 25–40% after about 10 pore volumes of the ethanol–water mixture had been flowed. Additional analyses using a higher-spatial-resolution x-ray system are needed to determine the presence and extent of microcracking in the clay due to dewatering.

Acknowledgments

This work was performed under the auspices of the U.S. Department of Energy by the University of California Lawrence Livermore National Laboratory under Contract Number W-7405-ENG-48 and supported specifically by the Office of Basic Energy Science and the Environmental Management Science Program of the Office of Environmental Management and the Office of Energy Research. The following people are gratefully acknowledged for their assistance: E. Carlberg, D. Rikard, B. Ralph, and C. Boro, who provided technical support; C. Talaber, T. Carey, and E. Chen, who provided editorial assistance; and B. Bonner, who provided stimulating discussion that helped this work.

References

Anandarajah, A., 2003, Mechanism controlling permeability change in clays due to changes in pore fluid: J. Geotech. Geoenviron. Eng., **129**, 163–172.

Archie, G.E., 1942, The electrical resistivity log as an aid in determining some reservoir characteristics: Trans. Am. Inst. Mining, Metallurgical, and Petroleum Engineers, **146**, 54–62.

Brown, K.W., and Thomas, J.C., (??) A mechanism by which organic liquids increase the hydraulic conductivity of compacted clay materials: Soil Sci. Am. J., **51**, 1451–1459.

Chan, C.Y., Buettner, H.M., Newmark, R., and Mavko, G., 2000, Conductivity measurements of sand–clay mixtures: A modified experimental method: J. Environ. Engin. Geophys., **5**, 15–26.

Dias, C.A., 2000, Developments in a model to describe low-frequency electrical polarization of rocks: Geophysics, **65**, 437–451.

Johnson, D.L., Koplik, J., and Schwartz, L.M., 1986, New pore-size parameter characterizing transport in porous media: Phys. Rev. Lett., **57**, 2564–2567.

Jones, D.P., 1997, Investigation of clay–organic reactions using complex resistivity: Ph.D. thesis, Colorado School of Mines.

Knight, R., 1984, The use of complex plane plots in studying the electrical response of rocks: J. Geomagnet. Geoelect., **35**, 767–776.

Macdonald, J. R., 1985, Generalizations of "universal dielectric response" and a general distribution-of-activation-energies model for dielectric and conducting systems: J. Appl. Phys., **58**, 1971–1978.

Olhoeft, G.R., 1985, Low-frequency electrical properties: Geophysics, **50**, 2492–2503.

Olhoeft, G.R., and King, T.V.V., 1991, Mapping subsurface organic compounds noninvasively by their reactions with clays: USGS Water Resources Investigation Report 91-4034.

Roberts, J.J., and Lin, W., 1997, X-ray radiography of fracture flow and matrix imbibition in Topopah Spring tuff under a thermal gradient: Int. J. Rock Mech. Mining Sci., **34**, 3–4, Paper No. 259.

Sen, P.N., and Goode, P.A., 1992, Influence of temperature on electrical conductivity on shaly sands: Geophysics, **57**, 89–96.

Sen, P.N., Goode, P.A., and Sibbit, A., 1988, Electrical conduction in clay-bearing sandstones at low and high salinities: J. Appl. Phys., **63**, 4832–4840.

Ward, S.H., and Hohmann, G.W., 1987, Electromagnetic theory for geophysical applications: *in* Electromagnetic Methods

in Applied Geophysics, Nabighian, M. (ed.), Society for Exploration Geophysics, Vol. 1, 131–311.

Waxman, M.H., and Smits, L.J.M., 1968, Electrical conductivities in oil-bearing shaly sands: Soc. Petrol. Eng. J., **8**, 107–122.

Wildenschild, D., Roberts, J.J., and Carlberg, E.D., 1999, Influence of microstructural properties on geophysical measurements in sand–clay mixtures: Symposium on the Application of Geophysics to Engineering and Environmental Problems.

Wildenschild, D., Roberts, J.J., and Carlberg, E.D., 2000, Electrical properties of sand–clay mixtures: The effect of microstructure: Geophys. Res. Lett., **27**, 3085–3089.